

ICRF Heating in Helical Reactor

Kenji SAITO, Tetsuo SEKI, Ryuhei KUMAZAWA, Hiroshi KASAHARA, Fujio SHIMPO,
Goro NOMURA and Takashi MUTOH

National Institute for Fusion Science, 322-6 Oroshi-cho, Toki 509-5292, Japan

(Received 8 January 2009 / Accepted 8 July 2009)

ICRF heating is a favorable high-density plasma heating method, since the ICRF wave can propagate in high-density plasma. ICRF heating in a helical reactor was calculated by using an antenna code and a ray tracing code assuming high-density plasma without resonance layers of α -particles in the plasma core. Enough loading resistance and a low electric field inside the ICRF antenna was obtained. Strong heating of plasma is expected in high-density plasma by heating electron and tritium, especially with the configuration of the second harmonic resonance layer of tritium on the magnetic axis shifted onto the saddle point.

© 2010 The Japan Society of Plasma Science and Nuclear Fusion Research

Keywords: ICRF heating, helical reactor, LHD, α -particle, ray tracing, ELD/TTMP, second harmonic heating

DOI: 10.1585/pfr.5.S1030

1. Introduction

Helical fusion reactors [1, 2] have the advantage of steady-state operation, since there is no need for a current drive. Before ignition in the helical reactor, the plasma must be heated by external heating such as ion cyclotron range of frequencies (ICRF) heating, electron cyclotron heating (ECH) and neutral beam injection (NBI). ICRF heating is a favorable high-density plasma heating method, since the fast wave launched from the ICRF antenna can be transmitted to the plasma core, even in high-density plasma. In a Large Helical Device (LHD) [3], ions were efficiently heated by minority ion heating (hydrogen as minority ions, helium as majority ions), especially by locating the ion cyclotron resonance layer on the saddle point of magnetic field strength where the gradient of the magnetic field strength is zero, which is characteristic of the helical device [4]. An injected energy of 1.6 GJ was achieved, mainly using this heating method [5]. Mode conversion heating is also an efficient heating method, although the heating deposition is far off-axis around the normalized minor radius of 0.73 [4]. However, there are problems with ICRF heating in reactors. One problem is the induced loss of fusion-produced α -particles caused by the interaction between marginally passing α -particles and the RF wave [6]. Another problem is the existence of evanescence of the fast wave in the vacuum region between the plasma and ICRF antennas.

In section 2, resonance configurations to reduce the induced loss of α -particles will be shown. In section 3, calculations of the loading resistance and electric field in the ICRF antenna will be shown. Ray tracing analysis is conducted in section 4, while section 5 presents the summary.

2. Candidate of Frequency and Magnetic Field Strength in Helical Reactor

It was shown by the Monte Carlo simulation that α -particles are well confined without an RF field [7]. We propose configurations in which the second harmonic resonance layer of tritium locates at the plasma core and the resonance layers of α -particles locate out of the plasma core to reduce the induced loss of α -particles by RF waves. Figure 1-a shows the ion cyclotron resonance layers at the vertically elongated toroidal section, where $f = nf_{ci}$ ($n = 1, 2$). The magnetic configuration is the same with that of LHD ($R_{ax} = 3.75$ m, vacuum), except for the scale factor of 3.5. The magnetic field strength on axis B_{ax} is 4.92 T and the RF frequency f is 50 MHz. The second harmonic resonance layers of α -particles do not exist inside the last closed flux surface, and only the fundamental resonance layer locates in the high-field peripheral region of the plasma. Therefore, loss of high-energy α -particles

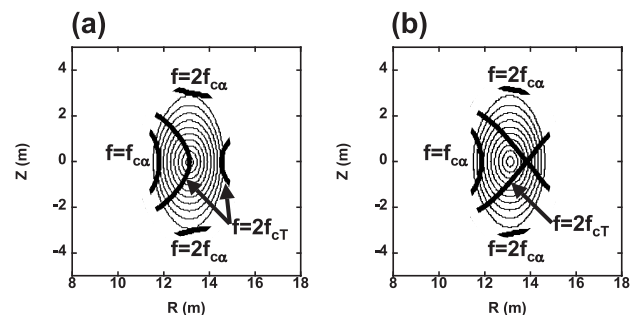


Fig. 1 Configurations of ion cyclotron resonance layers. (a) Resonance layer of tritium on magnetic axis ($f = 50$ MHz, $B_{ax} = 4.92$ T). (b) Resonance layer of tritium on saddle point ($f = 50$ MHz, $B_{ax} = 5.10$ T).

author's e-mail: saito@nifs.ac.jp

by the RF field is expected to be reduced, and the energy of α -particles will be sufficiently utilized for plasma heating and the heat load by the α -particles on divertor plates or first wall will be kept low. A second harmonic resonance layer of tritium locates on the magnetic axis, therefore tritium heating by the cyclotron damping and electron heating by the electron Landau damping (ELD) / transit-time magnetic pumping (TTMP) are expected. Figure 1-b shows the resonance layers in the case of $B_{ax} = 5.10$ T and $f = 50$ MHz. The fundamental α -particle resonance slightly approaches the plasma core. The resonance layer of tritium does not locate on the magnetic axis, but instead at the saddle point, where efficient ion heating is expected.

3. Calculation of ICRF Antenna Performance

The loading resistance and the electromagnetic field around the ICRF antenna were calculated by using the variational method [8]. In this calculation, the slab model of plasma was used and an infinite area of the Faraday shield and back-plate was assumed. Waves launched from the antenna never return to the antenna. A simplified dielectric tensor of cold plasma was used, where a component of the electric field along the magnetic field line was zero. The size of the model antenna was 600 mm in strap width, 1000 mm in strap height, 50 mm between the Faraday shield and the strap, and 350 mm between the strap and the back-plate. A large distance of 500 mm between the plasma and the Faraday shield was assumed to avoid the intense heat load on the ICRF antenna. The RF frequency was 50 MHz and the magnetic field strength was 4.5 T (constant). A parabolic density profile was assumed with the peak density of $2 \times 10^{20} \text{ m}^{-3}$. The ion species were deuterium and tritium with the same concentration. Power was fed into the two straps of the upper and lower antenna by the coaxial lines with the characteristic impedance Z_c of 50Ω through an outer port at the vertically elongated toroidal section assuming FFHR-2S [2], since it is not necessary to use a blanket area for the feed lines. By the calculation, it was found that the loading resistance R was 10Ω in the case of the opposite current direction on straps. Assuming maximum voltage in the coaxial line V_{\max} of 70 kV, which is twice of the interlock level in LHD, the allowable injection power by two antennas was estimated to be 19.6 MW by using the equation

$$\text{Power} = \frac{1}{2} R \left(\frac{V_{\max}}{Z_c} \right)^2. \quad (1)$$

The electric field inside the antenna was also calculated. The strength of the electric field between the Faraday shield and the strap was the largest. In the case of 19.6 MW injection, it was 8.1 kV/cm, smaller than that of breakdown for $E \perp B$ (> 30 kV/cm) [9]. Figure 2-a shows the intensity of the component of the Poynting vector directed to plasma. The peaks are located near the antenna tips. In

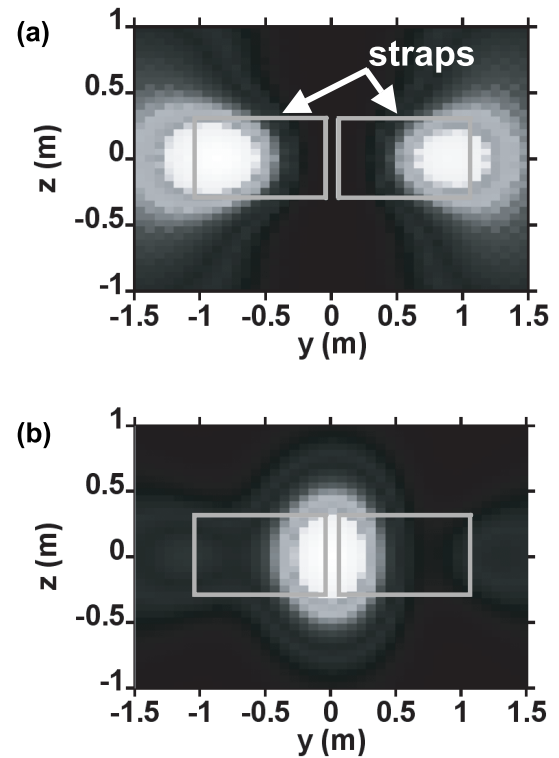


Fig. 2 Intensity of the component of Poynting vector directed to plasma at the plasma edge. The y -axis is the direction of the antenna current, and the z -axis is the direction of the magnetic field. The straps are connected to the coaxial lines at $y = \pm 0.05$ m and grounded at $y = \pm 1.05$ m. (a) Opposite current direction case. (b) Same current direction case.

the case of the same current direction on straps, a loading resistance of 9.5Ω and power of 18.6 MW is possible. The maximum electric field was 14.2 kV/cm, which was still at the allowable level. The peak of intensity of the Poynting vector was located between the antennas, as shown in Fig. 2-b.

4. Ray Tracing Calculation of ICRF Wave in Helical Reactor

The ray tracing calculation was conducted using the peaks of the Poynting vector obtained in section 3 as initial positions since the intensity of the Poynting vector is localized as shown in Figs. 2-(a) and (b). The wave number vector projected on a flux surface is written as

$$\vec{k}_{\text{surf}} = \vec{k}_{//} + \vec{k}_{\perp \text{surf}}, \quad (2)$$

where $\vec{k}_{//}$ is the parallel wave number vector to the magnetic field line and $\vec{k}_{\perp \text{surf}}$ is the perpendicular component of the projected wave number vector on the flux surface,

$$\vec{k}_{//} = (\vec{k} \cdot \vec{b})\vec{b}, \quad \vec{k}_{\perp \text{surf}} = (\vec{k} \cdot \vec{e})\vec{e}, \quad (3)$$

$$\vec{b} = \frac{\vec{B}}{|\vec{B}|}, \quad \vec{e} = \vec{b} \times \frac{\nabla \rho}{|\nabla \rho|}, \quad (4)$$

where \vec{k} is the wave number vector and ρ is the normalized minor radius. The magnitude of \vec{k}_{surf} should be less than $2\pi f/c \approx 1 \text{ m}^{-1}$, since the wide evanescent region exists between the ICRF antenna and the plasma. Moreover, $k_{\parallel} = 0$ should be avoided to prevent the equation of absorption from dispersing. Therefore, four initial values of the wave number of $(k_{\parallel 0}, k_{\perp \text{surf}0}) = (-0.7 \text{ m}^{-1}, -0.7 \text{ m}^{-1}), (-0.7 \text{ m}^{-1}, 0.7 \text{ m}^{-1}), (0.7 \text{ m}^{-1}, -0.7 \text{ m}^{-1}), (0.7 \text{ m}^{-1}, 0.7 \text{ m}^{-1})$ were selected for the ray tracing calculation where k_{surf} is small but k_{\parallel} is not 0. In this calculation, a magnetic field configuration of LHD was used with the scale factor of 3.5. The dielectric tensor of cold plasma was used for the calculation of ray trajectory and polarization. Absorbed power was calculated by using the absorption rate Q and the wave energy W ,

$$Q = \frac{\epsilon_0}{2} \omega \vec{E}^* \cdot \vec{K}^a \cdot \vec{E}, \quad (5)$$

$$W = \frac{1}{4\mu_0} \vec{B}^* \cdot \vec{B} + \frac{\epsilon_0}{4} \vec{E}^* \cdot \frac{\partial \omega \vec{K}^h}{\partial \omega} \cdot \vec{E}, \quad (6)$$

where \vec{E} is the polarized electric field and \vec{K} is the hot plasma dielectric tensor. The absorbed power was superposed with the same weight ignoring the effect of interference. High density plasma with an internal diffusion barrier (IDB) [10] with the following profiles of electron density and temperatures of ions and electrons were supposed,

$$n_e = n_{e0} [0.8 \exp\{-(\rho/0.35)^{2.5}\} + 0.1(1 - \rho^{6.5}) + 0.1], \quad (7)$$

$$T_{i,e} = T_{i,e0}(1 - \rho^4). \quad (8)$$

Deuterium and tritium was the same concentration, and the fusion products and impurities were ignored. Ion and electron temperatures on the magnetic axis $T_{i,e0}$ were 8 keV. The electron density on the magnetic axis n_{e0} was scanned from $1 \times 10^{20} \text{ m}^{-3}$ to $5 \times 10^{20} \text{ m}^{-3}$ supposing high-density ignition.

4.1 Opposite current direction on straps

A ray tracing calculation was conducted from two initial positions where the strength of the Poynting vector shown in Fig. 2-a is the maximum in the case of the opposite current direction on straps. The resonance layer of tritium located on the magnetic axis, as shown in Fig. 1-a. Figures 3-a and b show an example of ray trajectory where the initial $(k_{\parallel}, k_{\perp \text{surf}})$ was $(0.7 \text{ m}^{-1}, 0.7 \text{ m}^{-1})$ and the electron density on the magnetic axis was $3 \times 10^{20} \text{ m}^{-3}$. The wavelength is only 0.5 m even at the start point, which is much smaller than the plasma minor radius ($\approx 2 \text{ m}$), therefore ray tracing is applicable. The ray bounced at a R -cutoff in the plasma edge. Figure 4-a shows the variation of k_{\parallel} . In spite of the small initial k_{\parallel} , it was enlarged, especially with the high electron density. The large k_{\parallel} up-shift is characteristic to helical devices, as pointed out in Ref. [11]. The large k_{\parallel} is preferable for the direct electron heating by ELD/TTMP, since the components

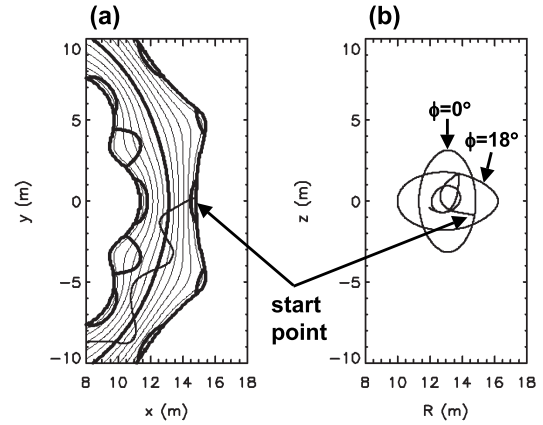


Fig. 3 An example of ray trajectory with the initial wave number $(k_{\parallel 0}, k_{\perp \text{surf}0})$ of $(0.7 \text{ m}^{-1}, 0.7 \text{ m}^{-1})$ and the initial position (x_0, y_0, z_0) of $(14.7 \text{ m}, 0.9 \sin(10^\circ) \text{ m}, -0.9 \cos(10^\circ) \text{ m})$ assuming inclined magnetic field line by 10° around the x -axis. (a) Top view with the flux surfaces and the resonance layers on mid plane. (b) Relation between R ($= \sqrt{x^2 + y^2}$) and z with the plasma shapes at the vertically elongated toroidal section ($\phi = 0^\circ$) and the horizontally elongated toroidal section ($\phi = 18^\circ$).

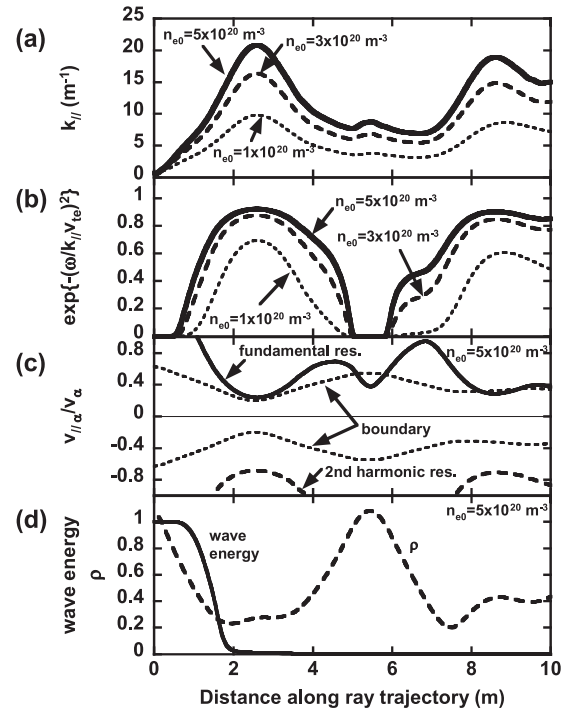


Fig. 4 (a) Variation of k_{\parallel} for three electron densities on magnetic axis. (b) Variation of $\exp\{-(\omega/k_{\parallel} v_{te})^2\}$ as an index of ELD/TTMP intensity. (c) Resonance condition of α -particles. v_{α} is the birth velocity of α -particles. 'boundary' means normalized v_{\parallel} of marginally passing α -particles with the birth energy (3.52 MeV). (d) Wave energy and normalized minor radius.

for the electron heating of \vec{K}^a (anti-Hermitian part of \vec{K}) are proportional to $\exp\{-(\omega/k_{\parallel} v_{te})^2\}$. In Fig. 4-b, the val-

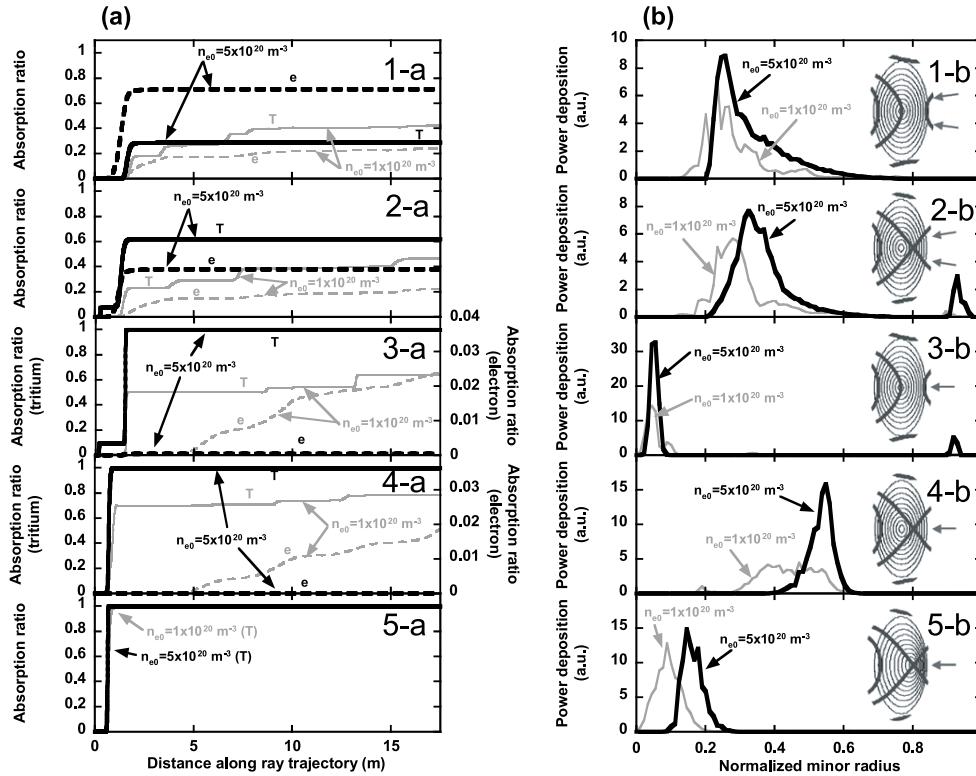


Fig. 5 (a) Absorbed wave energy by electron and tritium normalized by initial wave energy for various initial positions and resonance configurations. (b) Deposited power density multiplied by $dV/d\rho$, where V is the plasma volume inside a flux surface. At the right side, initial positions and resonance configurations are shown.

ues of $\exp\{-(\omega/k_{\parallel}v_e)^2\}$ for different electron densities are shown, and it increases with k_{\parallel} . Figure 4-c shows the resonance condition of α -particles with the energy of 3.52 MeV for the largest k_{\parallel} case of $n_{e0} = 5 \times 10^{20} \text{ m}^{-3}$ calculated by the equation of the Doppler effect,

$$\omega - n\omega_{ce} = k_{\parallel}v_{\parallel\alpha, \text{res}}, \quad (9)$$

where n is the harmonic number. The wave interacted with passing α -particles, but before the interaction with marginally passing α -particles, it was enough damped, as shown in Fig. 4-d.

Figure 5-1-a shows the integrated absorbed energy by electron and tritium normalized by initial wave energy. Absorption increased with the plasma density, and the portion of absorption by electron and tritium was changed. Wave energy was absorbed mainly by tritium at low density, whereas wave energy was absorbed mainly by electrons at high density, since before the cyclotron resonance of tritium, electrons start to absorb wave energy due to enhanced electron heating at high density. Figure 5-1-b shows the power deposition profile. The location of the power deposition is a little off-axis ($\rho \approx 0.25$). Figure 5-2-a shows the absorbed energies in the case of resonance on the saddle point. In this case, the ratio of tritium heating increased, since rays experienced the resonance of tritium earlier. Therefore, the deposition profile shifted outward, as shown in Fig. 5-2-b.

4.2 Same current direction on straps

The initial position was set at the outer edge on the mid-plane at the vertically elongated toroidal section, since the Poynting vector was maximum there in the case of the same current direction on straps, as shown in Fig. 2-b. Ray tracing was conducted for two cases of resonance of tritium on the magnetic axis and the saddle point. As shown in Fig. 5-3-a, in the case of resonance on the axis, tritium heating was dominant and power was deposited on the magnetic axis (Fig. 5-3-b). One-pass absorption was small when the density was low. However, by the configuration of the resonance layer of tritium on the saddle point, one-pass absorption of the low density plasma increased, although the peak of deposition shifted around $\rho = 0.5$, as shown in Figs. 5-4-a and 5-4-b. Therefore, the configuration of the magnetic axis on the saddle point may be useful for intense core heating when the density is low. The magnetic axis was shifted onto the saddle point artificially, and the resonance layer of tritium was located on the axis. It resulted in the intense core heating by tritium, as shown in Figs. 5-5-a and 5-5-b. The second harmonic heating was thought to be enhanced by the effects of the large wave number perpendicular to the magnetic field line around the axis and the low gradient of the magnetic field strength at the saddle point. Due to the strong absorption by tritium, electrons were not heated. Since the wave energy is sufficiently absorbed at the magnetic axis before the increasing of k_{\parallel} , the acceleration of α -particles will be avoided.

5. Summary

To reduce the induced loss of α -particles by RF waves, the configurations without the cyclotron resonance layer of the α -particles in plasma core were selected as candidates for ICRF heating in a helical reactor. The second harmonic resonance layer of tritium was located at the plasma core. The ICRF antenna for the helical reactor was not optimized, but the large loading resistance of 10Ω and the high power injection of 20 MW from two antennas were found to be achievable in spite of the large distance of 500 mm between plasma and antennas. By the calculation of ray tracing, it was found that the wave number parallel to the magnetic field line was greatly up-shifted, especially in high-density IDB plasma, even if the initial wave number was small, which enabled ELD/TTMP heating. The configuration of the second harmonic resonance layer on the magnetic axis shifted onto the saddle point makes the intense core heating possible.

Acknowledgements

The authors would like to thank Dr. H. Okada of

Kyoto University for his theoretical support of the antenna calculation with the variational method.

- [1] A. Sagara *et al.*, Fusion Eng. Des. **83**, 1690 (2008).
- [2] N. Yanagi *et al.*, *Proposal of Split and Segmented-type Helical Coils for the Heliotron Fusion Energy Reactor*, Proceedings of 18th International Toki Conference (2008).
- [3] O. Motojima *et al.*, Nucl. Fusion **47**, S668 (2007).
- [4] K. Saito *et al.*, Nucl. Fusion **41**, 1021 (2001).
- [5] K. Saito *et al.*, J. Nucl. Mater. **363-365**, 1323 (2007).
- [6] D.S. Darrow *et al.*, PPPL Reports, PPPL-3164 (1996).
- [7] S. Murakami *et al.*, Fusion Sci. Technol. **46**, 241 (2004).
- [8] K. Theilhaber and J. Jacquinot, Nucl. Fusion **24**, 541 (1984).
- [9] S.J. Wukitch *et al.*, 2002 Proc. 19th Int. Conf. on Fusion Energy 2002 (Lyon, France, 2002) (Vienna: IAEA) CD-ROM file FT/P1-14 and <http://www.iaea.org/programmes/ripe/physics/fec2002/html/fec2002.htm>
- [10] N. Ohya *et al.*, Plasma Phys. Control. Fusion **48**, B383 (2006).
- [11] N. Takeuchi *et al.*, J. Plasma Fusion Res. SERIES **6**, 642 (2004).